

FreeMan: Towards Benchmarking 3D Human Pose Estimation in the Wild

Jiong Wang^{1,2*}, Fengyu Yang^{1*}, Wenbo Gou¹, Bingliang Li¹, Danqi Yan¹,
Ailing Zeng³, Yijun Gao², Junle Wang², Ruimao Zhang^{1†}

¹The Chinese University of Hong Kong, Shenzhen ²Tencent ³IDEA

jiongwang@link., fengyuyang@link., zhangruimao@cuhk.edu.cn

Abstract

Estimating the 3D structure of the human body from natural scenes is a fundamental aspect of visual perception. This task carries great importance for fields like AIGC and human-robot interaction. In practice, 3D human pose estimation in real-world settings is a critical initial step in solving this problem. However, the current datasets, often collected under controlled laboratory conditions using complex motion capture equipment and unvarying backgrounds, are insufficient. The absence of real-world datasets is stalling the progress of this crucial task. To facilitate the development of 3D pose estimation, we present FreeMan, the first large-scale, real-world multi-view dataset. FreeMan was captured by synchronizing 8 smartphones across diverse scenarios. It comprises 11M frames from 8000 sequences, viewed from different perspectives. These sequences cover 40 subjects across 10 different scenarios, each with varying lighting conditions. We have also established an automated, precise labeling pipeline that allows for large-scale processing efficiently. We provide comprehensive evaluation baselines for a range of tasks, underlining the significant challenges posed by FreeMan. Further evaluations of standard indoor/outdoor human sensing datasets reveal that FreeMan offers robust representation transferability in real and complex scenes. FreeMan is now publicly available at <https://wangjiong.github.io/freeman>.

1 Introduction

Estimating 3D human poses from real scene input is a longstanding yet active research topic since its huge potential in real applications, such as animation creation [1, 2], virtual reality [3, 4], the metaverse [5–7] and human-robot interaction [8]. Specifically, it aims to identify and determine the spatial positions and orientations of the human body’s parts in 3D space from input data such as the image or the video. Despite numerous models proposed in recent years [9–11], practical implementation in real scenes remains challenging due to the viewpoint variability, occasions, human scale variation and complex background. Some challenges may stem from the disparity between the recent benchmarks and real-world scenarios. As shown in Fig. 1, the widely recognized Human3.6M [12], along with the currently largest dataset HuMMAn [13], are usually collected in laboratory settings utilizing intricate equipment, which maintains constant camera parameters and offers minimal variation in background conditions. The effectiveness of the trained models when trained using these datasets often experiences a significant decline in real-world environments.

From a data-oriented perspective, we have identified several constraints that hinder the performance of the existing models. **(1) Insufficient Scene Diversity.** Existing datasets, as shown in Tab. 2, are mainly collected in controlled laboratory conditions, which may not be optimal for robust model training due to static lighting conditions and uniform backgrounds. This limitation becomes especially

*The first two authors contributed equally to this work. Email: {jiongwang, fengyuyang}@link.cuhk.edu.cn

†The corresponding author is Ruimao Zhang. Email: zhangruimao@cuhk.edu.cn



Figure 1: The left displays sample frames from Human3.6M [12] and HuMMAN [13], which were collected under laboratory conditions, and contrasted with our FreeMan dataset that was collected in real-world scenarios. Frames from FreeMan have been cropped into a square format for visualization purposes, with the original resolution being 1920×1080 pixels. The right-hand side demonstrates the test results on 3DPW of the HMR model [16] when trained on these three datasets. Notably, the model trained using FreeMan is able to adapt flawlessly to real-world conditions, demonstrating its superior generalization ability.

Dataset	Environment	#Subj	#Action	#Scen	#Seq	#Frame	#Camera	FPS
HumanEval[17]	Laboratory	4	6	1	168	80K	7	30
CMU Panoptic[18]	Laboratory	8	5	1	65	154M	31	30
MPI-INF-3DHP[19]	Real Scene	8	8	1	16	1.3M	14	30
3DPW[15]	Real Scene	7	47	4	60	51K	1	30
Mirrored Human[20]	Laboratory	-	-	-	-	1.5M	1	30
Human3.6M[12]	Laboratory	9	15	1	840	3.6M	4 (Fixed)	30
AIST+{21}	Laboratory	30	10	1	1408	10.1M	9 (Fixed)	30
HuMMAN[13]	Laboratory	1000	500	1	400K	60M [†]	11 (Fixed)	30
HuMMAN-released[13]	Laboratory	132	20	1	4466	278K [‡]	11 (Fixed)	30
FreeMan	Real Scene	40	123	10 [§]	8000	11.3M	8 (Movable)	30 / 60

¹ Comparison of our proposed FreeMan dataset with existing 3D Human Pose datasets. Only HD Cameras counted for CMU Panoptic[18].

[†] Only 1% of the HuMMAN dataset (600K frames) is made publicly available.

[‡] FreeMan includes 10 types of scenes that correspond to 29 locations. Fixed means cameras are fixed within the whole dataset, while our cameras are movable and camera poses vary among video sequences.

Figure 2: Overview of Datasets



Figure 3: Equipment setting of data collection using 8 cameras.

crucial when the objective is to estimate 3D pose in real-world scenarios, where scene contexts exhibit substantial variability. In certain datasets, even though the data is collected from outdoor scenes, *e.g.*, MuCo [14] and 3DPW [15] in Tab. 2, the variety of scenarios remains remarkably limited. This constraint significantly hampers the applicability of trained models across a broader range of situations. **(2) Limited Actions and Body Scales.** In existing datasets, the range of human actions tends to be rather limited. Even in the currently largest dataset, HuMMAN [13], the variety of actions in the publicly available data is quite restricted. Additionally, these large datasets typically employ fixed cameras to capture data from various perspectives. The distance from the camera to the actor is relatively constant, which results in a relatively fixed human body scale across different videos. **(3) Restricted Scalability.** The annotation of current datasets primarily relies on expensive manual processing, which greatly restricts the scalability of the datasets. Especially when the camera used for collection is movable, how to effectively align data from different cameras and perform efficient annotation remains an open issue.

To address these above issues, this work presents FreeMan, a novel large-scale benchmark for 3D human pose estimation in the wild. FreeMan contains 11M frames in 8000 sequences captured by 8 smartphone cameras from different views simultaneously, as illustrated in Fig. 3. It covers 40 subjects in 10 kinds of scenes. To our best knowledge, it is the current largest multi-view 3D pose estimation dataset, with variable camera parameters and complex background environments. It is 215 \times of the famous outdoor dataset 3DPW [15]. From a practical perspective, it has several appealing strengths: **Firstly**, a large number of scenes introduce diversity in both backgrounds and lighting, enhancing the generalizability of models trained on FreeMan in real-world scenarios. This makes it particularly suitable for evaluating algorithmic performance in practical applications. **Secondly**, the distances between the 8 cameras and the actors are variant (*i.e.*, 2 to 5.5 meters) both within and among subjects, resulting in significant scale changes in human bodies across different sequences. **Thirdly**, although we employed mobile data collection devices, the annotation of the FreeMan dataset does not rely on costly manual processes, thereby significantly enhancing the scalability of the dataset. **Lastly**, the proposed FreeMan encompasses a wide range of pose estimation tasks, which include monocular 3D estimation, 2D-to-3D lifting, multi-view 3D estimation, and neural rendering of human subjects.

We present thorough evaluation baselines for the aforementioned tasks on FreeMan, highlighting the inherent challenges of such a new benchmark.

In summary, this paper has made three contributions: (1) We have constructed a large-scale dataset for 3D human pose estimation in uncontrolled environments. The impressive transferability of the models trained on this dataset to real-world scenarios has been demonstrated. (2) We have showcased a simple yet effective toolchain that enables the automatic generation of precise 3D annotations from the collected data. (3) We provide comprehensive benchmarks for human pose estimation and modeling on FreeMan, facilitating downstream applications. These baselines highlight potential directions for future algorithmic enhancements.

2 Related Work

Human Pose Datasets. Human modeling is a significant task in computer vision. Existing datasets predominantly rely on 2D and 3D keypoint annotations, with 3D keypoint datasets available in two forms: monocular and multi-view. For 2D keypoint, there are some single-frame datasets such as MPII [22] and COCO [23], which provide diverse images with 2D keypoints annotations, while video datasets such as J-HMDB [24], Penn Action [25] and PoseTrack [26] provide 2D keypoints with temporal information. In contrast, 3D keypoint datasets are often constructed in indoor scenes, such as Human3.6M [12], CMU Panoptic [27], MPI-INF-3DHP [19], AIST++ [28] and HuMMAn [13] for multi-view. There also exists some outdoor datasets such as 3DPW [15] for monocular cases. Details of these datasets are shown in Tab. 2. However, the majority of outdoor datasets such as MPI-INF-3DHP, MuCo-3DHP, and 3DPW exhibit a limited variety of acquisition scenes, and the datasets that involve fixed camera poses such as AIST++.

3D Human Pose Estimation. The present study categorizes the task of 3D pose estimation into three distinct types, namely 2D-to-3D pose lifting, monocular 3D pose estimation, and multi-view 3D pose estimation. In the 2D-to-3D pose lifting task, Martinez [29] proposed a simple baseline to regress the 3d keypoints based on a convolutional neural network from 2D keypoints. However, subsequent works, such as Videopose3D[30], PoseFormer[31] and MHFormer[10], have improved upon this baseline by integrating temporal information into their models. In monocular 3D pose estimation task, HMR[16], SPIN[32] takes a single RGB image as input to perform 3D human pose estimation, which is often used as baselines for comparison with other algorithms, such as PARE[9], SPEC[33] and HybrIK[34]. Additionally, multi-view methods are proposed to accommodate potential body parts overlapping in monocular view. Iqbal’s [35] and MCSS [36] adopt weak supervision to reduce the dependence on the 3D annotated pose, while Canonpose [37] and EpipolarPose [38] turned to self-supervise fashion to deal with multi-view data.

Neural Rendering of Human Subjects. With the development of NeRF[39] in dynamic scene rendering, people also focus on the dynamic rendering of humans. Compared to dynamic scenes, the non-rigid property of humans has more challenges. The prior knowledge of body movements can provide a good prior for rendering, and many methods use SMPL[40] as a prior for body rendering. Most methods reconstruct human bodies through multi-view videos[41–43], while recent works have also employed single-view videos, such as HumanNeRF[44], FlexNeRF[45], YOTO[46].

3 FreeMan Dataset

FreeMan is a large-scale multi-view dataset in the wild, offering precise 3D pose annotations. It comprises $11M$ frames from 1000 sessions, featuring 40 subjects across 10 types of scenes. The dataset includes $10M$ frames recorded at 30FPS and an additional $1M$ frames at 60FPS. Next, we highlight the diversity of FreeMan, from various camera settings and scenario selections

Scenarios. We design 10 types of real-world scenes, comprising 4 indoor and 6 outdoor scenes, for our data collection. Fig. 4 illustrates the scene diversity of our FreeMan. The blue section represents the data collected outdoors, while the red sector refers to frames captured in indoor scenes. Specifically, there are 2.76 million frames captured indoors and 8.45 million frames captured outdoors. Additionally, there are different frame numbers collected under varying lighting conditions, with 1 million frames captured at night and 7.45 million frames captured during the day outdoors. Moreover, the central block of the circle denotes different scenarios, while the blocks on the outermost circle refer to actions. The areas of the blocks are proportional to the corresponding frame numbers. For more details about the distribution of scenarios, please refer to the supplementary material.

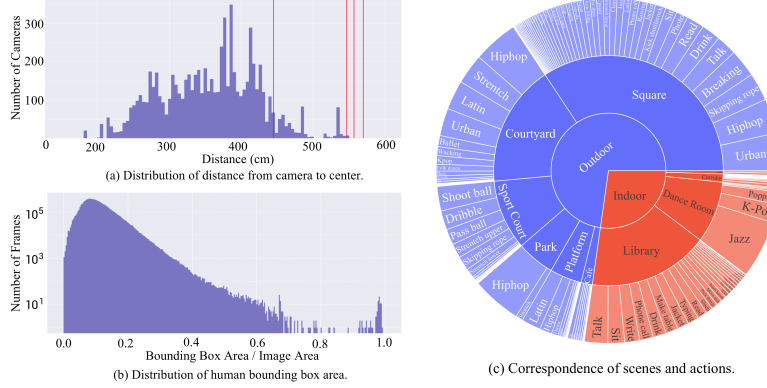


Figure 4: (a) Distribution of distance from the camera to the center of the system, indicated by translation along the z-axis in camera parameters. Four vertical red lines represent the distance of 4 cameras in Human3.6M [12]. (b) Distribution of human bounding box areas. The horizontal axis represents the ratio of the bounding box area over the image area. The vertical axis is in log scale. (c) Correspondence of scenes and actions. Areas of blocks represent the scale of the respective frame number. The outmost circle shows actions and the circle in the middle present 10 type of scenes in our dataset. Zoom in 10× for the best view.

Action Set. Following the popular action recognition dataset NTU-RGBD120[47], we compose our action set with several common actions corresponding to scenes in daily life, *e.g.*, drinking and talking in a cafe and reading in the library. Also, subjects interact with real objects to make actions as close to real life as possible. As shown in the topmost row of Fig. 5, interaction with objects brings complicated occlusions, making our data more challenging. For outdoor scenarios, we set the data collection field as large as possible to help subjects perform actions with little restriction.

Camera Poses. Cameras in previous 3D human pose datasets [13, 12, 18] are fixed during data collection, resulting that only a few camera poses being included. As shown in Fig. 3, Our cameras are attached to lightweight tripods and are newly placed from time to time, and translation from the center of the system to camera d , which is the physical distance between the camera and the system center, can vary from 2m to 5.5m. Fig. 4 (a) shows the distribution of d and the corresponding number of cameras. Most cameras are located around 4 meters far away from the system center. Besides, we show the distribution of the human bounding box area in Fig. 4 (b), in a unit of ratio to the whole image area, to demonstrate the variation of human size. With variations in camera translation and human actions, the area of human bounding boxes varies from 0.01 to 0.7 of the whole image area.

Subjects. There are 40 subjects participating in the construction of FreeMan and recruitment is completely based on voluntary. All of them are well-informed and signed the agreement to make the data public for research purposes only.

4 Data Acquisition & Annotation Pipeline

Overview. To collect a large-scale dataset from real-world environments, we developed a comprehensive toolchain, as shown in Fig. 6. Unlike previous toolchains used in controlled or idealized conditions, we carefully accounted for potential challenges in outdoor settings, including calibration and synchronization errors. To overcome these issues, we incorporated automated correction procedures to ensure efficient data collection.

4.1 Hardware Setup

Cameras. We collect FreeMan via 8 Mi11 phones [48] indexed from 1 to 8 as our data collection devices. **Note 8 collection of one action as one session, which corresponds to RGB sequences from 8 views.** and each phone is attached to a tripod to keep stable within each data collection session.

As shown in Fig. 3, all devices are positioned in a circle around a human at a height of approximately 1.6 meters above the ground, with the distance from the camera to the system center varying from 2 to 5.5 meters. which is similar to real-life usage scenarios. Each smartphone captures RGB sequences using the main camera at 1920×1080 resolution and 30/60 FPS. During the data collection process,



Figure 5: The diverse frames in FreeMan. The topmost two rows illustrate a range of indoor and outdoor scenes, highlighting the diversity of scene contexts, lighting conditions, and subjects. The third row exhibits frames from different cameras, showcasing the variance across views. The final row illustrates the temporal variation of human poses from a consistent viewpoint, emphasizing the dynamism of motion capture.

actors perform actions facing the device with odd-numbered indices. As shown in Fig. 6(a), the only requirement beyond devices is to connect all devices to the same server stably.

Camera Calibration. At the beginning of each session, we calculate the intrinsic and extrinsic camera parameters in two steps with a chessboard tiled at the center of the system, following the standard implementation in OpenCV[49, 50]. We attach cameras to tripods and collect tiled chessboards from each view. In this phase, chessboard frames from all views are sent to the server and the server detects corner points, calculates camera extrinsic parameters of each device, and sends parameters back to cameras. Cameras are allowed for the next step only if extrinsic parameters are received.

Device Synchronization. Previous works [13, 12, 18] have synchronized devices using wired interfaces in a laboratory. However, the complexity of the entire system coupled with the difficulty in deploying it in real-world environments, has prompted us to consider alternative methods. To address issues related to usability and device constraints, we connect all devices wirelessly to a single server and developed an Android app that utilizes the Network Time Protocol (NTP) [51] to calculate the time difference between each device and the server’s clock. During the capture process, time information is stored locally on each device as a timecode, while the server records the synchronized capture interval for all devices. The starting frame is determined by matching the timecode to the frame closest to the server’s clock time. This approach ensures device synchronization, with synchronization errors limited to smaller than a single frame during our testing. At frame rates of 30FPS and 60FPS, this corresponds to 33ms and 16ms, respectively.

4.2 Pose Annotation.

After camera calibration, subjects enter the capture area to perform actions. Once videos are collected, we use a state-of-the-art detector YOLOX[52] to detect human locations and HRNet-w48[53] to detect 2D keypoints of 8 views $K_{2D} \in \mathbb{R}^{8 \times 17 \times 2}$ in COCO[23] format. To eliminate the effect of potential wrong keypoints output, keypoint predictions with confidence lower than a threshold ϕ are removed. Then remaining 2D keypoints are used for triangulation to get 3D human pose $K_{3D} \in \mathbb{R}^{17 \times 3}$ with pre-computed camera parameters. Here, we set ϕ to be 0.5. Furthermore, we optimize K_{3D} with smoothness constraints and bone length constraints introduced in HuMMan[13] resulting in optimized 3D pose $\tilde{K}_{3D} \in \mathbb{R}^{17 \times 3}$. Then we fit a standard SMPL[40] model to the estimated 3D skeleton by SMPLify [54] to produce a rough mesh annotation. After that, we project 3D keypoints to 2D image

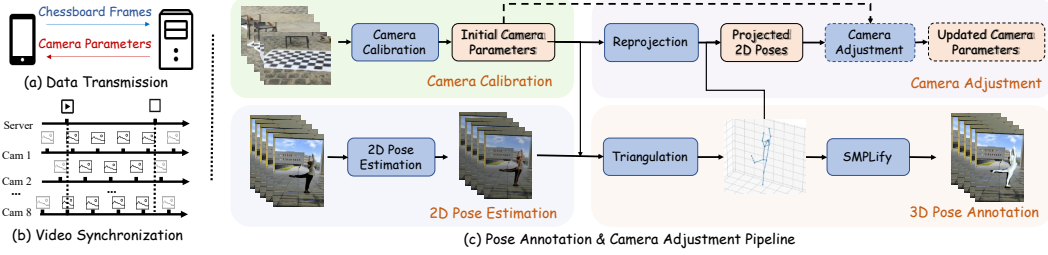


Figure 6: The illustration of data collection and annotation toolchain: (a) depicts the transmission of signals between cameras and servers for camera calibration, where chessboard frames are sent to the server, and camera parameters are returned. (b) demonstrates the synchronization process among devices. (c) showcases the pipeline for annotation and camera adjustment.



Figure 7: The examples of human pose annotations are presented as follows. In the left part, the first row displays 2D keypoints directly generated by HRNet-w48 [53], while the second row illustrated the re-projected 2D poses. When HRNet fails to deal with occlusions, our toolchain automatically corrects annotations by incorporating multi-view priors. The right part showcases the SMPL annotation examples for each view in our dataset.

planes of each view using corresponding camera parameters. With regularization in triangulation and optimization along the temporal axis, the re-projected 2D poses \tilde{K}_{2D} is a refined version compared with K_{2D} . Comparison between original K_{2D} and \tilde{K}_{2D} are shown in the left part of Fig. 7.

Camera Adjustment. Finally, for cameras that failed in calibration accidentally, we adjust camera parameters through pose computation[55] if needed. If more than two cameras failed in calibration, the session is discarded directly. Otherwise, we ignore the uncalibrated views first, then triangulate the remaining 2D poses into 3D poses. We can obtain the camera parameters of uncalibrated cameras by minimizing the re-projection error of 2D-3D point correspondences.

4.3 Annotation Quality Assessment

To demonstrate the effectiveness of our toolchain, we test the toolchain on Human3.6M[12]. We select 3 different actions of each subject in the training set, which covers 10% sequences of the whole training set and all kinds of actions. Performance is assessed by Euclidean distance between estimated 2D poses and ground truth 2D poses in units of pixels. The error results in 9.9 pixels for images with the size of 1000×1000 , demonstrating that our toolchain can generate accurate annotations.

To validate the effectiveness of camera adjustment for failure cases in calibration, we randomly mask a camera for all sessions and use the other 3 views to get 3D poses, then compute the parameters of the missing one via pose computation. Then 3D poses are projected to the corrupted view by estimated camera parameters, mean error between resulting 2D poses and ground truth is 7.42 pixels.

5 Benchmarks

We have constructed four benchmarks utilizing images and annotations derived from our dataset. The data is subdivided based on subjects, allocating 18 subjects for training, 7 for validation, and 15 for testing purposes. This partitioning results in three subsets composed of $5.87M$, $700K$, and $3.69M$ frames, respectively. For each benchmark, subject lists of each subset are shared, and only views selected from the session vary for each task. **(1) Monocular 3D Human Pose Estimation (HPE).** This task involves taking an RGB image or sequence from a monocular view as input and

predicting 3D coordinates relative to the camera. For this benchmark, we randomly select one view from each session to construct the dataset. The performance of algorithms is measured by widely used Mean Per Joint Position Error (MPJPE)[12] and Procrustes analysis MPJPE (PA-MPJPE)[40]. **(2) 2D-to-3D Lifting.** Given that 2D human poses can be predicted using existing 2D keypoint detectors [56–58, 53], the primary goal of this task is to effectively elevate these 2D poses into the 3D space within the camera coordinate system. The evaluation metrics are the same as HPE. **(3) Multi-View 3D Human Pose Estimation.** Due to occlusions in motion capture, monocular methods often encounter difficulties. Estimating the 3D human pose from multiple views presents a natural solution to overcome this problem. For this task, models are provided with images or videos from multiple views, along with corresponding camera parameters. The objective is to predict the 3D coordinates of human joints in the same world coordinate system as the cameras. The performance is measured by MPJPE and average precision (AP) following previous work[59]. **(4) Neural Rendering of Human Subjects.** The free-viewpoint rendering of humans is a significant issue in human modeling. With the rise in popularity of neural radiance fields (NeRF) [39] for the novel view rendering task, several methods, including HumanNeRF [44], have emerged. These methods utilize monocular human motion videos as input to synthesize novel views of dynamic humans through NeRF. The widely used metrics of prediction are PSNR, SSIM[60] and LPIPS[61].

6 Experiments

We experiment with the four benchmarks. In human 3D pose estimation tasks, we conduct several transfer tests with other standard datasets to evaluate the effectiveness and transferability of our proposed FreeMan dataset. Existing similar datasets, Human3.6M[12] & HuMMAn[13], are used for comparison. Since *HuMMAn* only releases 1% of data, we only involve it in monocular 3D human pose estimation and 2D-to-3D lifting. In the neural rendering of human subjects tasks, we train the model from one of the 8 views and test from the rest of the views in selected sessions.

6.1 Monocular 3D Human Pose Estimation

Train	Supervision	Test	HMR		PARE	
			MPJPE	PA	MPJPE	PA
Human3.6M	2D+3D KPTs	3DPW	279.92	133.13	118.54	81.22
HuMMAn	2D+3D KPTs	3DPW	407.57	192.75	110.99	63.11
HuMMAn	2D KPTs+SMPL	3DPW	475.73	184.15	114.20	66.19
HuMMAn	2D+3D KPTs+SMPL	3DPW	437.52	203.17	114.33	72.12
FreeMan	2D+3D KPTs	3DPW	157.46	87.93 ^{↑33.95%}	118.31	68.72 ^{↑15.39%}
FreeMan	2D KPTs+SMPL	3DPW	151.85	88.85 ^{↑51.75%}	94.27	60.39 ^{↑8.76%}
FreeMan	2D+3D KPTs+SMPL	3DPW	159.31	91.33 ^{↑55.04%}	98.33	64.51 ^{↑10.55%}

Table 1: Monocular 3D HPE performance of HMR[16] and PARE[9] trained on different dataset for monocular Human Pose Estimation. PA stands for PA-MPJPE and both metrics are in unit of millimeters. The lower metrics is, the better performance model obtains. All released part of HuMMAn is used for training. \uparrow refers to the improvement relative to HuMMAn and \uparrow refers to the improvent relative to Human3.6M.

Implementation details. For the Human3.6M [12] and HuMMAn [13] datasets, all views in their training set are utilized. In contrast, for FreeMan, we randomly sample a single view from sessions in the training split, resulting that the frame numbers of all three datasets being $312K$, $253K$, and $233K$, respectively. To enhance efficiency, videos of all three datasets are downsampled to 10FPS, following the implementation of MMpose [62]. We trained HMR[16] and PARE[9] models on different datasets using configurations open-sourced by [63]. Please refer to Appendix for more.

Results. We perform testing on the test set of 3DPW [15]. The performance of the models trained on different datasets, with varying types of supervision, are reported in Tab. 1. Notably, the HMR models trained on FreeMan exhibit significantly better performance on the 3DPW test set compared to those trained on Human3.6M and HuMMAn with PA-MPJPE 133.13mm and 192.75mm respectively, which indicates that FreeMan demonstrates superior generalizability compared to the others. The same results are obtained with PARE, further confirming that our FreeMan outperforms even in more advanced algorithms. This can be attributed to the diversity of scene contexts and human actions present in our dataset, which provides better transferability in real-world scenarios.

Train	Test	AP@25mm (%) ↑	AP@50mm (%) ↑	AP@75mm (%) ↑	AP@100mm (%) ↑	Recall@500mm (%) ↑	MPJPE@500mm (mm) ↓
Human3.6M	Human3.6M	32.32	97.47	98.61	98.99	100.00	25.29
Human3.6M	FreeMan	0.00	0.00	0.00	0.00	0.06	89.85
Human3.6M	FreeMan (w/ GT Root)	0.00	1.27	11.44	21.40	96.20	103.02
FreeMan	FreeMan	43.38	88.77	97.73	99.12	99.97	26.07
FreeMan	Human3.6M	0.00	5.77	82.85	92.62	96.68	61.29
FreeMan	Human3.6M (w/ GT Root)	0.00	6.60	87.91	95.38	100.00	58.30

Table 2: Multi-View 3D Pose Estimation results of VoxelPose[59]. Ground truth root position (GT Root) is not used if not specified. Recall@500mm shows the percentage that falls within the threshold, and the MPJPE@500mm indicates the average MPJPE values within the threshold. Rows highlighted shows the best setting in cross-domain test.

6.2 Multi-View 3D Human Pose Estimation

Implementation Details. We conduct in-domain and cross-domain tests between Human3.6M and FreeMan to evaluate the effectiveness and generalization ability. We conduct the experiments of multi-view 3D human pose estimation with VoxelPose[64], which locates the human root first and then regresses 3D joint location accordingly. COCO-format poses in FreeMan are transformed to match that in Human3.6M via interpolation. We trained VoxelPose[64] on the two datasets following official implementation. For Human3.6M, bounding box annotations are from [65] and its validation set is used for the test. For FreeMan, we only use videos of odd-indexed views from the training set.

Results. Results of all experiments are reported in Tab. 2. For in-domain testing, the model trained on FreeMan achieves MPJPE@500mm of 26.61mm on test set consisting of *odd-indexed* views. For cross-domain testing, the model trained on FreeMan achieves Recall@500mm of 96.68% while MPJPE@500mm is 62.37mm on Human3.6M validation set. However, the model trained on the Human3.6M dataset fails to locate human on FreeMan test set. To get rid of the effects of root location, we input the ground truth root locations to model directly. With this setting, the model trained on Human3.6M obtains MPJPE@500mm of 154.41mm on FreeMan test set, while the model trained on FreeMan can obtain MPJPE@500mm of 58.30mm on Human3.6M validation set. Results show that the model trained on FreeMan has a much better generalization ability, while that on Human3.6M struggles in transfer testing.

6.3 2D-to-3D Pose Lifting

Implementation Details. We employ four methods, either CNN-based or Transformer-based, including SimpleBaseline[29], VideoPose3D[30], PoseFormer[31] and MHFormer[10] in this task, and all the methods follow the corresponding official implementation. The results of VideoPose3D and PoseFormer can be found in Appendix. For training set in this task, we select one view from every session and down-sample the videos to 15FPS, resulting in the frame number to be 350K, which is similar to the amount of released part of HuMMAN (253K) and much smaller than Human3.6M (1500K). In order to verify the generalization across datasets, we unify the test set to be AIST++[28]. To verify the effect of the dataset scale, we also train our model on the whole training set.

Results. The experimental results are shown in Tab. 3. Results of the in-domain test on FreeMan are provided as a baseline for future work. For in-domain testing, the MPJPE of SimpleBaseline trained on FreeMan (79.22mm) is larger than that on HuMMAN[13] (78.5mm) and Human3.6M[12] (53.4mm), demonstrating that FreeMan is a more challenging benchmark. Besides, all the methods trained on FreeMan tend to generalize better than that on HuMMAN and Human3.6M when testing on AIST++ under the same setting. Although the scale of FreeMan training set is of a similar magnitude as HuMMAN’s, which is much smaller than Human3.6M’s, models trained on FreeMan outperform models trained on the other two by a large margin. Furthermore, when the training set is expanded to all frames in training split, FreeMan can further boost models to achieve better performance, proving that our large-scale data helps to improve model performance.

6.4 Neural Rendering of Human Subjects.

Implementation Details. We employ 10 scenes captured by FreeMan to train HumanNeRF[44], a deep neural network that aims to achieve high-quality human-centric new synthesis. To obtain human body segmentation annotations, we utilize the SAM (Segment Anything)[66] algorithm using our bounding boxes as prompts. Throughout the training step, we randomly select one view for each session and render the rest 7 view as novel views for testing. We then calculate metrics including PSNR, SSIM, and LPIPS, to evaluate the performance of the model. Please refer to Appendix for results of data at 60FPS.

Results. The reconstruction results in 10 scenes are shown in Tab. 4. The best reconstruction achieves a high PSNR of 30.11 which indicates FreeMan contains contents that the model can learn and fit very well. While the performance varies, the lowest PSNR of 23.86 shows FreeMan also contains contents that are outside of model’s learning scope and challenging. Additionally, the results in 10 scenes including both familiar contents that the model can handle well and more challenging new contents demonstrates the diversity of our dataset.

Algorithm	Train	Test	MPIPE (mm)	PA (mm)
SimpleBaseline	FreeMan	FreeMan	90.53	54.17
	FreeMan [†]	FreeMan	79.22	49.11
	Human3.6M	AIST++	212.57	138.98
	HuMMAN	AIST++	255.5	116.86
	FreeMan	AIST++	156.96	105.85 ^{↑10.30%}
	FreeMan [†]	AIST++	126.23	88.07 ^{↑11.04%}
MHFormer	FreeMan	FreeMan	93.00	63.50
	FreeMan [†]	FreeMan	77.06	53.38
	Human3.6M	AIST++	171.19	133.37
	HuMMAN	AIST++	188.73	101.52
	FreeMan	AIST++	132.99	88.79 ^{↑12.54%}
	FreeMan [†]	AIST++	124.34	79.22 ^{↑21.07%}

Table 3: Performance of methods with different training and testing datasets in 2D-to-3D Pose Lifting. PA stands for PA-MPJPE. [†] refer to experiments with the whole training set of FreeMan. Smaller MPIPE and PA-MPJPE indicate better performance. Highlighted rows show training on our dataset achieves the best performance in the transfer test. [↑] refers to the improvement relative to HuMMAN.

Scene	PSNR \uparrow	SSIM \uparrow	LPIPS* \downarrow
Square	25.98	0.9501	58.38
Corridor	24.57	0.9340	81.39
Sports Port	26.33	0.9662	30.09
Park	23.86	0.9439	73.61
Courtyard	28.56	0.9630	53.99
Dance Room	30.11	0.9658	43.34
Library	29.41	0.9665	31.53
Platform	26.79	0.9439	70.01
Lobby	25.41	0.9387	78.80
Cafe	27.32	0.9644	37.88

Table 4: Neural rendering results by using HumanNeRF[44] on 10 scenes of FreeMan. Note that LPIPS* = LPIPS $\times 10^3$.

7 Conclusion

We present FreeMan, a novel large-scale multi-view 3D pose estimation dataset with comprehensive tasks and 3D human pose annotations. We elaborately develop a simple yet effective annotation pipeline to automatically annotate frame-level 3D landmarks and precise 3D human motions at a much lower cost. We establish benchmarks covering multiple tasks in human modeling, including monocular and multi-view 3D human pose estimation, 2D-to-3D pose lifting, and neural rendering of human subjects. Extensive experimental results demonstrate the strengths of the proposed FreeMan.

Limitation and future work. While we have validated the superiority of our dataset on numerous in-domain and cross-domain cases, there is still a wide range of potential applications that are worth exploring. Additionally, since the data is automatically annotated, more evaluation schemes for the accuracy of annotations and understanding their potential impact on downstream applications remain open issues. We consider these aspects as future work for further investigation. As a large-scale human motion dataset, our FreeMan addresses the existing gap between the current datasets and real-scene applications, and we are optimistic that it will catalyze the development of algorithms designed to model and sense human behavior in real-world scenes.

References

- [1] Chung-Yi Weng, Brian Curless, Pratul P. Srinivasan, Jonathan T. Barron, and Ira Kemelmacher-Shlizerman. Humannerf: Free-viewpoint rendering of moving people from monocular video. In *Proceedings of the IEEE/CVF Conference on Computer Vision and Pattern Recognition (CVPR)*, pages 16210–16220, June 2022.
- [2] Jae Shin Yoon, Lingjie Liu, Vladislav Golyanik, Kripasindhu Sarkar, Hyun Soo Park, and Christian Theobalt. Pose-guided human animation from a single image in the wild. In *Proceedings of the IEEE/CVF Conference on Computer Vision and Pattern Recognition*, pages 15039–15048, 2021.
- [3] Thomas Waltemate, Dominik Gall, Daniel Roth, Mario Botsch, and Marc Erich Latoschik. The impact of avatar personalization and immersion on virtual body ownership, presence, and emotional response. *IEEE Transactions on Visualization and Computer Graphics*, 24(4):1643–1652, 2018.
- [4] Shivam Grover, Kshitij Sidana, and Vanita Jain. Pipeline for 3d reconstruction of the human body from ar/vr headset mounted egocentric cameras. *arXiv preprint arXiv:2111.05409*, 2021.

- [5] Lik-Hang Lee, Tristan Braud, Pengyuan Zhou, Lin Wang, Dianlei Xu, Zijun Lin, Abhishek Kumar, Carlos Bermejo, and Pan Hui. All one needs to know about metaverse: A complete survey on technological singularity, virtual ecosystem, and research agenda. *arXiv preprint arXiv:2110.05352*, 2021.
- [6] Jae Shin Yoon. Metaverse in the wild: Modeling, adapting, and rendering of 3d human avatars from a single camera. 2022.
- [7] Doina Popescu Ljungholm. Metaverse-based 3d visual modeling, virtual reality training experiences, and wearable biological measuring devices in immersive workplaces. *Psychosociological Issues in Human Resource Management*, 10(1), 2022.
- [8] Abdelfetah Bentout, Mustapha Aouache, Abderraouf Maoudj, and Isma Akli. Human–robot interaction in industrial collaborative robotics: a literature review of the decade 2008–2017. *Advanced Robotics*, 33(15-16):764–799, 2019.
- [9] Muhammed Kocabas, Chun-Hao P. Huang, Otmar Hilliges, and Michael J. Black. PARE: part attention regressor for 3d human body estimation. *CoRR*, abs/2104.08527, 2021.
- [10] Wenhao Li, Hong Liu, Hao Tang, Pichao Wang, and Luc Van Gool. Mhformer: Multi-hypothesis transformer for 3d human pose estimation. *CoRR*, abs/2111.12707, 2021.
- [11] Tao Wang, Jianfeng Zhang, Yujun Cai, Shuicheng Yan, and Jiashi Feng. Direct multi-view multi-person 3d human pose estimation. *Advances in Neural Information Processing Systems*, 2021.
- [12] Catalin Ionescu, Dragos Papava, Vlad Olaru, and Cristian Sminchisescu. Human3.6m: Large scale datasets and predictive methods for 3d human sensing in natural environments. *IEEE Transactions on Pattern Analysis and Machine Intelligence*, 36(7):1325–1339, jul 2014.
- [13] Zhongang Cai, Daxuan Ren, Ailing Zeng, Zhengyu Lin, Tao Yu, Wenjia Wang, Xiangyu Fan, Yang Gao, Yifan Yu, Liang Pan, Fangzhou Hong, Mingyuan Zhang, Chen Change Loy, Lei Yang, and Ziwei Liu. HuMMAn: Multi-modal 4d human dataset for versatile sensing and modeling. In *17th European Conference on Computer Vision, Tel Aviv, Israel, October 23–27, 2022, Proceedings, Part VII*, pages 557–577. Springer, 2022.
- [14] Dushyant Mehta, Oleksandr Sotnychenko, Franziska Mueller, Weipeng Xu, Srinath Sridhar, Gerard Pons-Moll, and Christian Theobalt. Single-shot multi-person 3d pose estimation from monocular rgb. In *3D Vision (3DV), 2018 Sixth International Conference on*. IEEE, sep 2018.
- [15] Timo Von Marcard, Roberto Henschel, Michael J Black, Bodo Rosenhahn, and Gerard Pons-Moll. Recovering accurate 3d human pose in the wild using imus and a moving camera. In *Proceedings of the European conference on computer vision (ECCV)*, pages 601–617, 2018.
- [16] Angjoo Kanazawa, Michael J. Black, David W. Jacobs, and Jitendra Malik. End-to-end recovery of human shape and pose. In *Computer Vision and Pattern Recognition (CVPR)*, 2018.
- [17] Leonid Sigal, Alexandru O. Balan, and Michael J. Black. Humaneva: Synchronized video and motion capture dataset and baseline algorithm for evaluation of articulated human motion. *Int. J. Comput. Vis.*, 87(1-2):4–27, 2010.
- [18] Tomas Simon Hanbyul Joo, HaoLiu Xulong Li, LinGui Lei Tan, and Timothy Godisart Sean Banerjee. Panoptic studio: A massively multiview system for social interaction capture. *IEEE Transactions on Pattern Analysis and Machine Intelligence*, 41(1), 2019.
- [19] Dushyant Mehta, Helge Rhodin, Dan Casas, Pascal Fua, Oleksandr Sotnychenko, Weipeng Xu, and Christian Theobalt. Monocular 3d human pose estimation in the wild using improved cnn supervision. In *3D Vision (3DV), 2017 Fifth International Conference on*. IEEE, 2017.
- [20] Qi Fang, Qing Shuai, Junting Dong, Hujun Bao, and Xiaowei Zhou. Reconstructing 3d human pose by watching humans in the mirror. In *CVPR*, 2021.
- [21] Rui long Li, Shan Yang, David A. Ross, and Angjoo Kanazawa. Learn to dance with aist++: Music conditioned 3d dance generation, 2021.

- [22] Mykhaylo Andriluka, Leonid Pishchulin, Peter Gehler, and Bernt Schiele. 2d human pose estimation: New benchmark and state of the art analysis. In *IEEE Conference on Computer Vision and Pattern Recognition (CVPR)*, June 2014.
- [23] Tsung-Yi Lin, Michael Maire, Serge J. Belongie, Lubomir D. Bourdev, Ross B. Girshick, James Hays, Pietro Perona, Deva Ramanan, Piotr Dollár, and C. Lawrence Zitnick. Microsoft COCO: common objects in context. *CoRR*, abs/1405.0312, 2014.
- [24] H. Jhuang, J. Gall, S. Zuffi, C. Schmid, and M. J. Black. Towards understanding action recognition. In *International Conf. on Computer Vision (ICCV)*, pages 3192–3199, December 2013.
- [25] Weiyu Zhang, Menglong Zhu, and Konstantinos G. Derpanis. From actemes to action: A strongly-supervised representation for detailed action understanding. In *2013 IEEE International Conference on Computer Vision*, pages 2248–2255, 2013.
- [26] Mykhaylo Andriluka, Umar Iqbal, Anton Milan, Eldar Insafutdinov, Leonid Pishchulin, Juergen Gall, and Bernt Schiele. Posetrack: A benchmark for human pose estimation and tracking. *CoRR*, abs/1710.10000, 2017.
- [27] Hanbyul Joo, Hao Liu, Lei Tan, Lin Gui, Bart Nabbe, Iain Matthews, Takeo Kanade, Shohei Nobuhara, and Yaser Sheikh. Panoptic studio: A massively multiview system for social motion capture. In *ICCV*, 2015.
- [28] Ruilong Li, Shan Yang, David A. Ross, and Angjoo Kanazawa. Learn to dance with aist++: Music conditioned 3d dance generation, 2021.
- [29] Julieta Martinez, Rayat Hossain, Javier Romero, and James J. Little. A simple yet effective baseline for 3d human pose estimation. *CoRR*, abs/1705.03098, 2017.
- [30] Dario Pavllo, Christoph Feichtenhofer, David Grangier, and Michael Auli. 3d human pose estimation in video with temporal convolutions and semi-supervised training. *CoRR*, abs/1811.11742, 2018.
- [31] Ce Zheng, Sijie Zhu, Matías Mendieta, Taojiannan Yang, Chen Chen, and Zhengming Ding. 3d human pose estimation with spatial and temporal transformers. *CoRR*, abs/2103.10455, 2021.
- [32] Nikos Kolotouros, Georgios Pavlakos, Michael J. Black, and Kostas Daniilidis. Learning to reconstruct 3d human pose and shape via model-fitting in the loop. In *Proceedings of the IEEE International Conference on Computer Vision*, 2019.
- [33] Muhammed Kocabas, Chun-Hao P. Huang, Joachim Tesch, Lea Müller, Otmar Hilliges, and Michael J. Black. SPEC: seeing people in the wild with an estimated camera. *CoRR*, abs/2110.00620, 2021.
- [34] Jiefeng Li, Chao Xu, Zhicun Chen, Siyuan Bian, Lixin Yang, and Cewu Lu. Hybrik: A hybrid analytical-neural inverse kinematics solution for 3d human pose and shape estimation. *CoRR*, abs/2011.14672, 2020.
- [35] Umar Iqbal, Pavlo Molchanov, and Jan Kautz. Weakly-supervised 3d human pose learning via multi-view images in the wild. In *Proceedings of the IEEE/CVF Conference on Computer Vision and Pattern Recognition*, pages 5243–5252, 2020.
- [36] Rahul Mitra, Nitesh B Gundavarapu, Abhishek Sharma, and Arjun Jain. Multiview-consistent semi-supervised learning for 3d human pose estimation. In *Proceedings of the ieee/cvf conference on computer vision and pattern recognition*, pages 6907–6916, 2020.
- [37] Bastian Wandt, Marco Rudolph, Petrißsa Zell, Helge Rhodin, and Bodo Rosenhahn. Canonpose: Self-supervised monocular 3d human pose estimation in the wild. In *Proceedings of the IEEE/CVF Conference on Computer Vision and Pattern Recognition*, pages 13294–13304, 2021.
- [38] Muhammed Kocabas, Salih Karagoz, and Emre Akbas. Self-supervised learning of 3d human pose using multi-view geometry. In *Proceedings of the IEEE/CVF conference on computer vision and pattern recognition*, pages 1077–1086, 2019.

- [39] Ben Mildenhall, Pratul P Srinivasan, Matthew Tancik, Jonathan T Barron, Ravi Ramamoorthi, and Ren Ng. Nerf: Representing scenes as neural radiance fields for view synthesis. *Communications of the ACM*, 65(1):99–106, 2021.
- [40] Matthew Loper, Naureen Mahmood, Javier Romero, Gerard Pons-Moll, and Michael J. Black. SMPL: A skinned multi-person linear model. *ACM Trans. Graphics (Proc. SIGGRAPH Asia)*, 34(6):248:1–248:16, October 2015.
- [41] Lingjie Liu, Weipeng Xu, Marc Habermann, Michael Zollhöfer, Florian Bernard, Hyeongwoo Kim, Wenping Wang, and Christian Theobalt. Neural human video rendering by learning dynamic textures and rendering-to-video translation. *arXiv preprint arXiv:2001.04947*, 2020.
- [42] Atsuhiro Noguchi, Xiao Sun, Stephen Lin, and Tatsuya Harada. Neural articulated radiance field. In *Proceedings of the IEEE/CVF International Conference on Computer Vision*, pages 5762–5772, 2021.
- [43] Chung-Yi Weng, Brian Curless, and Ira Kemelmacher-Shlizerman. Vid2actor: Free-viewpoint animatable person synthesis from video in the wild. *arXiv preprint arXiv:2012.12884*, 2020.
- [44] Chung-Yi Weng, Brian Curless, Pratul P Srinivasan, Jonathan T Barron, and Ira Kemelmacher-Shlizerman. Humannerf: Free-viewpoint rendering of moving people from monocular video. In *Proceedings of the IEEE/CVF Conference on Computer Vision and Pattern Recognition*, pages 16210–16220, 2022.
- [45] Vinoj Jayasundara, Amit Agrawal, Nicolas Heron, Abhinav Shrivastava, and Larry S Davis. Flexnerf: Photorealistic free-viewpoint rendering of moving humans from sparse views. In *Proceedings of the IEEE/CVF Conference on Computer Vision and Pattern Recognition*, pages 21118–21127, 2023.
- [46] Jaehyeok Kim, Dongyoon Wee, and Dan Xu. You only train once: Multi-identity free-viewpoint neural human rendering from monocular videos. *arXiv preprint arXiv:2303.05835*, 2023.
- [47] Jun Liu, Amir Shahroudy, Mauricio Perez, Gang Wang, Ling-Yu Duan, and Alex C Kot. Ntu rgb+ d 120: A large-scale benchmark for 3d human activity understanding. *IEEE transactions on pattern analysis and machine intelligence*, 42(10):2684–2701, 2019.
- [48] Mi11. <https://www.mi.com/global/product/mi-11/>, 2022.
- [49] G. Bradski. The OpenCV Library. *Dr. Dobb's Journal of Software Tools*, 2000.
- [50] Z. Zhang. A flexible new technique for camera calibration. *IEEE Transactions on Pattern Analysis and Machine Intelligence*, 22(11):1330–1334, 2000.
- [51] D.L. Mills. Internet time synchronization: the network time protocol. *IEEE Transactions on Communications*, 39(10):1482–1493, 1991.
- [52] Zheng Ge, Songtao Liu, Feng Wang, Zeming Li, and Jian Sun. Yolox: Exceeding yolo series in 2021. *arXiv preprint arXiv:2107.08430*, 2021.
- [53] Ke Sun, Bin Xiao, Dong Liu, and Jingdong Wang. Deep high-resolution representation learning for human pose estimation. In *CVPR*, 2019.
- [54] Federica Bogo, Angjoo Kanazawa, Christoph Lassner, Peter Gehler, Javier Romero, and Michael J. Black. Keep it SMPL: Automatic estimation of 3D human pose and shape from a single image. In *Computer Vision – ECCV 2016*, Lecture Notes in Computer Science. Springer International Publishing, October 2016.
- [55] Eric Marchand, Hideaki Uchiyama, and Fabien Spindler. Pose estimation for augmented reality: A hands-on survey. *IEEE Transactions on Visualization and Computer Graphics*, 22(12):2633–2651, 2016.
- [56] Zhe Cao, Tomas Simon, Shih-En Wei, and Yaser Sheikh. Realtime multi-person 2d pose estimation using part affinity fields. In *Proceedings of the IEEE conference on computer vision and pattern recognition*, pages 7291–7299, 2017.

- [57] Yilun Chen, Zhicheng Wang, Yuxiang Peng, Zhiqiang Zhang, Gang Yu, and Jian Sun. Cascaded pyramid network for multi-person pose estimation. In *Proceedings of the IEEE conference on computer vision and pattern recognition*, pages 7103–7112, 2018.
- [58] Hao-Shu Fang, Jiefeng Li, Hongyang Tang, Chao Xu, Haoyi Zhu, Yuliang Xiu, Yong-Lu Li, and Cewu Lu. Alphapose: Whole-body regional multi-person pose estimation and tracking in real-time. *IEEE Transactions on Pattern Analysis and Machine Intelligence*, 2022.
- [59] Hanyue Tu, Chunyu Wang, and Wenjun Zeng. Voxelpose: Towards multi-camera 3d human pose estimation in wild environment. In *European Conference on Computer Vision (ECCV)*, 2020.
- [60] Xiuming Zhang, Pratul P Srinivasan, Boyang Deng, Paul Debevec, William T Freeman, and Jonathan T Barron. Nerfactor: Neural factorization of shape and reflectance under an unknown illumination. *ACM Transactions on Graphics (TOG)*, 40(6):1–18, 2021.
- [61] Richard Zhang, Phillip Isola, Alexei A Efros, Eli Shechtman, and Oliver Wang. The unreasonable effectiveness of deep features as a perceptual metric. In *Proceedings of the IEEE conference on computer vision and pattern recognition*, pages 586–595, 2018.
- [62] MMPose Contributors. Openmmlab pose estimation toolbox and benchmark. <https://github.com/open-mmlab/mmpose>, 2020.
- [63] Hui En Pang, Zhongang Cai, Lei Yang, Tianwei Zhang, and Ziwei Liu. Benchmarking and analyzing 3d human pose and shape estimation beyond algorithms. In *Thirty-sixth Conference on Neural Information Processing Systems Datasets and Benchmarks Track*, 2022.
- [64] Hanyue Tu, Chunyu Wang, and Wenjun Zeng. Voxelpose: Towards multi-camera 3d human pose estimation in wild environment. In *European Conference on Computer Vision*, pages 197–212. Springer, 2020.
- [65] Haibo Qiu, Chunyu Wang, Jingdong Wang, Naiyan Wang, and Wenjun Zeng. Cross view fusion for 3d human pose estimation. In *Proceedings of the IEEE/CVF International Conference on Computer Vision*, pages 4342–4351, 2019.
- [66] Alexander Kirillov, Eric Mintun, Nikhila Ravi, Hanzi Mao, Chloe Rolland, Laura Gustafson, Tete Xiao, Spencer Whitehead, Alexander C Berg, Wan-Yen Lo, et al. Segment anything. *arXiv preprint arXiv:2304.02643*, 2023.
- [67] MMHuman3D Contributors. Openmmlab 3d human parametric model toolbox and benchmark. <https://github.com/open-mmlab/mmhuman3d>, 2021.
- [68] Haoyu Ma, Liangjian Chen, Deying Kong, Zhe Wang, Xingwei Liu, Hao Tang, Xiangyi Yan, Yusheng Xie, Shih-Yao Lin, and Xiaohui Xie. Transfusion: Cross-view fusion with transformer for 3d human pose estimation. *arXiv preprint arXiv:2110.09554*, 2021.
- [69] Kaiming He, Xiangyu Zhang, Shaoqing Ren, and Jian Sun. Deep residual learning for image recognition. In *Proceedings of the IEEE conference on computer vision and pattern recognition*, pages 770–778, 2016.

A Experiments

In this section, we present more details about experiments of benchmarks we set and provide further results of extensive experiments.

A.1 Monocular 3D Human Pose Estimation

For training of HMR[16], we use Adam optimizer with fixed learning rate of 2.5×10^{-4} . Training processes are conducted on a single NVIDIA RTX-3090-24GB GPU with batch size of 128. Additionally, for training of PARE[9], we use Adam optimizer with fixed learning rate of 5.0×10^{-5} at the backbone and head of the network. Training processes are conducted on a single NVIDIA RTX-3090-24GB GPU with batchsize of 128. Only 2D and 3D keypoints in FreeMan are converted to the format of *HumanData* provided in mmhuman3D[67].

We also make cross-dataset test on FreeMan, Human3.6M and HuMMan, the results of HMR on all test sets are shown in the Tab. 5. Based on the above advantages in FreeMan, it makes existing models more generalizable across datasets. And FreeMan is still challenging in in-domain experiments.

MPJPE/PA-MPJPE(mm)	Test	H36M	HuMMan	FreeMan
Train				
	H36M	98.62/59.17	392.89/175.94	350.97/178.85
	HuMMan	465.1/224.53	-	413.26/218.28
	FreeMan	192.19/112.7	302.09/147.67	148.22/100.56

Table 5: Cross-domain test results of HMR with the same supervision 2D&3D KPTs. MPJPE & PA-MPJPE are presented in unit of mm. Due to limited amount of data, all released part of HuMMan are used as training data.

A.2 2D-to-3D Pose Lifting

For training data in 2D-to-3D pose lifting, we use Human3.6M data provided by VideoPose3D[30], 70% of released data from HuMMan and training split of FreeMan, respectively. Following the original setting in HuMMan[13], we split released data of 100 subjects into training and test set by subjects. And test set of AIST++ and FreeMan are used for evaluation. During training, coordinates of 2D keypoints are normalized by height and width of corresponding images. Ground truth 3D poses are transferred into camera coordinate system and root of skeleton is placed to origin. During test, since resolution of images are different among datasets, input 2D keypoints are normalized by resolution of test images. Keypoints in COCO format are mapped to that in Human3.6M format following mmHuman3D[67].

All models are optimized using Adam optimizer with learning rate of 10^{-4} on one NVIDIA RTX-3090-24GB. SimpleBaseline[29], VideoPose3D[30] are trained for 80 epochs with batch size of 1024 and PoseFormer[31], MHFormer[10] are trained for 25 epochs with batch size of 256 following their original settings. We show the results of VideoPose3D and PoseFormer in Tab. 7.

A.3 Multi-view 3D Human Pose Estimation

In multi-view 3D human pose estimation, we use 4 views from both Human3.6M and FreeMan as input to VoxelPose. For Human3.6M, we follow the same processing steps as Transfusion[68]. For FreeMan, videos from odd-indexed views in training split are downsampled by 5 times to make data scale comparable. *Note single frame from all input views as one group*, Human3.6M and FreeMan include 223K and 132K groups of training data, respectively.

We first finetune ResNet-50[69] backbone pre-trained on COCO with each dataset for 10 epochs, and then optimized the latter modules in decoder for additional 15 epochs. Both the two stages use Adam optimizer with a learning rate of $1e - 4$ and batch size of 32. Models are trained on 4 NVIDIA A100-80GB GPUs. To solve the difference between joint definitions, we select 13 common joints between Human3.6M and COCO format, and then use the mid-points of the *left & right hips* and *left & right shoulders* to generate *mid-hip* and *neck*. In experiments, *mid-hip* is used as the root joint. The images are all cropped by human bounding boxes and then resized to make short edges the same.

Train	Test	Recall@500mm (%) ↑	MPJPE (mm) ↓
Human3.6M	Human3.6M	100	25.95
Human3.6M	FreeMan	0.06	-
Human3.6M	FreeMan (w/ GT Root)	96.20	154.41
FreeMan	FreeMan	99.97	26.61
FreeMan	Human3.6M	96.68	62.37
FreeMan	Human3.6M (w/ GT Root)	100.00	58.30
FreeMan	FreeMan [†]	99.98	35.04

Table 6: Results of VoxelPose[59] for Multi-View 3D Pose Estimation. Recall@500mm refer to ratio of predictions with MPJPE smaller than 500mm, MPJPE here has not threshold for all keypoints. FreeMan[†] represents test set of even indexed cameras. Ground truth root position (GT Root) is not used if not specified. Rows highlighted shows the best setting in cross-domain test.

Algorithm	Train	Test	MPJPE (mm)	PA (mm)
VideoPose3D	FreeMan	FreeMan	88.68	49.17
	FreeMan [†]	FreeMan	73.98	45.22
	Human3.6M	AIST++	190.46	146.98
	HuMMan	AIST++	265.10	125.56
	FreeMan	AIST++	146.66	99.01↑ _{21.15%}
	FreeMan [†]	AIST++	141.84	94.59↑ _{24.66%}
PoseFormer	FreeMan	FreeMan	92.94	64.91
	FreeMan [†]	FreeMan	77.68	54.39
	Human3.6M	AIST++	179.54	151.38
	HuMMan	AIST++	158.13	96.98
	FreeMan	AIST++	133.39	90.10↑ _{7.09%}
	FreeMan [†]	AIST++	133.89	84.68↑ _{14.52%}

Table 7: Performance of methods with different training and testing datasets in 2D-to-3D Pose Lifting. PA stands for PA-MPJPE. [†] refer to experiments with the whole training set of FreeMan. Smaller MPJPE and PA-MPJPE indicate better performance. Highlighted rows show training on our dataset achieves the best performance in the transfer test. ↑ refers to the improvement relative to HuMMan.

In Tab. 6, we report recall and MPJPE@500mm of each experiment. In calculation of Recall@500mm, only predictions with MPJPE smaller than 500mm are treated as positive predictions and a higher recall value refers to higher successful rate to locate humans in space. And only positive predicted poses contribute to MPJPE in the final column.

Without ground truth root location, the model trained on Human3.6M is unable to locate human in cross-domain test and thus corresponding MPJPE is not available. Even though the ground truth root positions are given, recall value and MPJPE of model trained on Human3.6M are still 96.20% and 103.02mm, which is lower than that of model trained on FreeMan in cross-domain test without GT root (96.68% & 61.29mm), demonstrating that our training set has better transferability and test set is more challenging.

A.4 Neural Rendering of Human Subjects

A.4.1 Implementation Details

We use 128 samples per ray and train for $400K$ iterations with the Adam optimizer as the setting in [44]. Samely, to improve the quality of our results, we have increased the number of rays sampled for the foreground subject, as identified by the segmentation masks. We achieve this by implementing a random ray sampling method that assigns a higher probability of 0.8 to foreground subject pixels and a lower probability of 0.2 to the background region. The resize scale of the image is set to 0.5. It takes about 48 hours to train on one NVIDIA RTX-3090-24GB for each one.

In order to ensure the quality of training, the number of frames of video clips in different scenes is in the interval of 300 to 1200 frames. The selected ten clips contain a variety of actions, ranging from slow and deliberate movements (such as warm-up exercises) to fast and energetic ones (such as dancing).

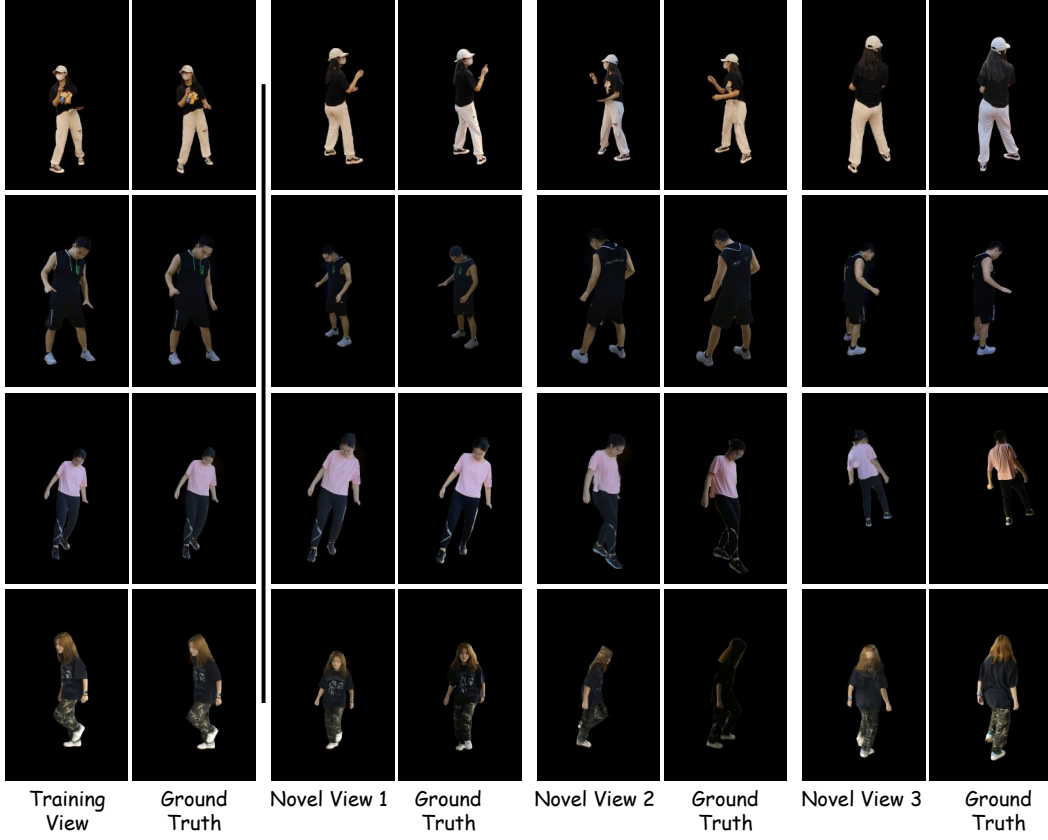


Figure 8: Rendering results in 30FPS dataset.

Scene	PSNR↑	SSIM↑	LPIPS* ↓
Square	23.99	0.9389	88.10
Park	24.43	0.9527	61.84

Table 8: Neural rendering in 60FPS results by using HumanNeRF[44]. Note that $LPIPS^* = LPIPS \times 10^3$.

A.4.2 Visualization Results

We show the visualization results of the reconstruction of the selected videos in FreeMan dataset at Fig. 8. The above two lines reflect the results of relatively good reconstruction, while the following two lines reflect the results of relatively poor reconstruction. This indicates that our FreeMan has sufficient diversity and challenges for NeRF reconstruction on human.

A.4.3 Experiments on 60FPS

Due to the occurrence of blur as Fig. 9 in body parts such as hands and feet when moving at high speeds, we collect videos at 60FPS to provide higher quality ground truth. We conduct experiments on two video clips from Park and Square scenes, and the experimental results are as Tab. 8. The results indicate that FreeMan remains highly challenging for human neural rendering in natural lighting conditions.



Figure 9: Example images of motion blur on human body in 30FPS dataset.

B Dataset Documentations

FreeMan is available for academic communities to boost related researches. Example code to load FreeMan in pytorch is open sourced at <https://github.com/wangjiongw/FreeMan> and data storage structure are illustrated in this section.

B.1 Data Format

Overall, FreeMan provided multi-view human motion data and corresponding 2D / 3D human pose annotations. All data are separated into videos, camera parameters, bounding boxes and keypoints annotations basd on data type. For each session, human motion videos of all views are stored in format of *mp4* and there are 8 synchronized videos for 8 views. Camera parameters, including image resolution, camera intrinsic parameters and camera extrinsic parameters, are saved in *JSON* format.

Human keypoint annotations are encoded into format of *npy*, which is also known as numpy array. 2D poses of one session are stored with an array whose shape is $[V, F, J, 2]$, where V for view indexes, F for frame number, J for total number of joints and keypoint locations are given by (x, y) coordinates in unit of pixels. 3D poses are stored in an array with shape of $[F, J, 3]$, and 3D keypoint locations are provided by (x, y, z) in world coordinate system.

B.2 Ethical Impact

All actors involved in FreeMan are recruited on basis of voluntary and well informed of data collection purpose. All volunteers signed a data collection agreement which declares project proposal and data to be released. To protect the privacy of all participants, we anonymized all data in the dataset by removing any personally identifiable information.

As FreeMan is constructed for research purpose only, FreeMan adopts license of CC BY-NC 4.0 (allowing non-commercial use only). Furthermore, subsequent users who are granted access to the dataset are required to sign relevant usage agreements and provide backup information. This is done to safeguard the privacy and security of individuals associated with the FreeMan dataset and prevent any misuse of the data.

B.3 Dataset Access

To access FreeMan data, users are required to sign a dataset usage agreement that illustrates responsibilities and requirements. After submitting signed agreement and basic information via online forms, they can download FreeMan from dataset host. All users should abide the relevant data use agreement and use rights will be terminated for any violations of data use agreement. The whole procedures can be found in <https://wangjiongw.github.io/freeman> and our data are uploaded to Huggingface and OpenXLab.